PHYSICAL REVIEW B **92**, 041202(R) (2015)

Exploring the origin of ultralow thermal conductivity in layered BiOCuSe

S. K. Saha*

Department of Physics, Indian Institute of Science, Bangalore 560012, India

(Received 15 December 2014; revised manuscript received 1 July 2015; published 15 July 2015)

Using first-principles density functional theory calculations, a systematic study of the lattice dynamics and related (e.g., dielectric and anharmonic) properties of BiOCuSe (bismuth-copper oxyselenide), along with a comparison with its isostructural analog LaOCuSe, is performed to find the origin of the ultralow thermal conductivity κ in BiOCuSe. From the marked differences in some of these properties of the two materials, the reasons why BiOCuSe is a better thermal insulator than LaOCuSe are elucidated. For this class of oxychalcogenide thermoelectrics, phonon frequencies with symmetries, characters, spectroscopic activities, displacement patterns, and pressure coefficients of different zone-center modes, dielectric constants, dynamical charges, and phonon and Grüneisen dispersions are also determined.

DOI: 10.1103/PhysRevB.92.041202 PACS number(s): 71.15.Mb, 63.20.−e, 73.50.Lw, 78.30.−j

BiOCuSe (also known as BiCuSeO or BiCuOSe)—a layered, transparent, p-type moderate band gap semiconductor composed of alternating insulating $(Bi_2O_2)^{2+}$ and conductive $(Cu_2Se_2)^{2-}$ layers—has attracted increasing attention since it was reported as a promising thermoelectric (TE) material in 2010 [1]. As TE materials are capable of generating electricity from waste heat, they are relevant to sustainable and renewable alternative energy solutions. The efficiency of TE devices is characterized by a dimensionless figure of merit, $ZT = \frac{S^2\sigma T}{\kappa}$, where S, σ, κ, and T are the Seebeck coefficient, electrical conductivity, thermal conductivity, and the absolute temperature, respectively [2]. Efforts to enhance the ZT involve increasing both S and σ, while decreasing κ [3]. Examples of these efforts include enhancement of S by designing quantum confinement effects [4], using electron energy barrier filtering [5], creating electronic resonance states [6], and reduction of κ by nanostructuring [7–10] and all-scale hierarchical architecturing [11], while maintaining carrier mobility by band energy alignment between the nanoprecipitate and matrix [12,13].

In the past four years, the TE performance (ZT) was significantly increased from 0.53 for pristine BiOCuSe to 1.4 [14] by optimization through dopants and texturation. More specifically, σ was increased by Sr doping [1], introducing Cu deficiencies [15], and Ba heavy metal doping [16,17]; for textured $Bi_{0.875}Ba_{0.125}CuSeO$ prepared by a hot-forging process, ZT reaches 1.4 at 923 K [14], which is the highest value reported so far for a bulk, lead-free, p-type material in this moderate temperature range [18].

The high ZT value of BiOCuSe largely outperforms that of other materials due to its intrinsically low κ in the temperature range of 300 K (∼0.9 W m $^{-1}$K^{-1}) to 923 K (∼0.45 W m^{-1}K^{-1}) [17]. This rapid decrease with temperature indicates that the heat in BiOCuSe is conducted primarily by phonons, as in other nonmetallic crystalline solids. Interestingly, the κ of BiOCuSe is observed to be four times lower than that of its isostructural analog, LaOCuSe [19]. Despite several years of research, surprisingly little is known about the main cause of its intrinsically low κ. It has recently been speculated that such low κ values are most likely a result of weak chemical bonds (Young's modulus, $Y \sim 78.8$ GPa [20]). However, among systems with the same crystal structure, it is very unlikely that the bonding strength would be very different. In such cases, the system with a heavier element is expected to exhibit lower thermal conductivity as a higher atomic mass is likely to produce lower phonon frequencies, stronger optical-acoustic scattering, and slower sound velocities.

Although a quantitative and comprehensive understanding of phonon dynamics is crucial to identify the reasons behind the lower κ in BiOCuSe and to find the best way to scatter, merge, or/and decay its phonons for phonon engineering, a theoretical investigation of its phonons is still lacking [21]. More regrettably, information (both theoretical and experimental) regarding its Born effective charge (BEC) and dielectric constant (DC) is missing in the literature. Motivated by these considerations, in this Rapid Communication, a systematic study of the lattice dynamics and related (viz., dielectric, elastic, and anharmonic) properties of BiOCuSe, together with a comparison to LaOCuSe, is performed using first-principles density functional theory (DFT) calculations with the Perdew-Burke-Ernzerhof for soild (PBEsol) functionals [22].

BiOCuSe and LaOCuSe (MOCuSe, M = Bi and La) belong to a class of layered materials that adopt the ZrSiCuAs type structure [see Fig. 1(a)] in the tetragonal $P4/nmm$ space group (No. 129) [28]. The PBEsol estimates of the equilibrium in-plane (out-of-plane) lattice spacings are $a = 3.9029$ ($c = 8.9186$) Å for BiOCuSe and $a = 4.0230$ ($c = 8.6509$) Å for LaOCuSe, in good agreement with the respective experimentally measured values of $a = 3.9213$ ($c = 8.9133$) Å for BiOCuSe and $a = 4.0670$ ($c = 8.8006$) Å for LaOCuSe. The same estimates of the Young's modulus for BiOCuSe and LaOCuSe are 93 and 101 GPa, respectively. Figure 1(b) shows the total and projected electronic density of states (EDOS) for BiOCuSe and LaOCuSe. It is immediately apparent that the BiOCuSe displays a significantly narrower gap (0.66 eV) than LaOCuSe (1.4 eV), consistent with optical measurements (the corresponding measured values are 0.75 eV [29] and 2.8 eV [30], respectively) [31].

As the MOCuSe unit cell consists of two formula units comprising eight atoms, there are 24 vibrational modes. At the

*sks.cmt@gmail.com

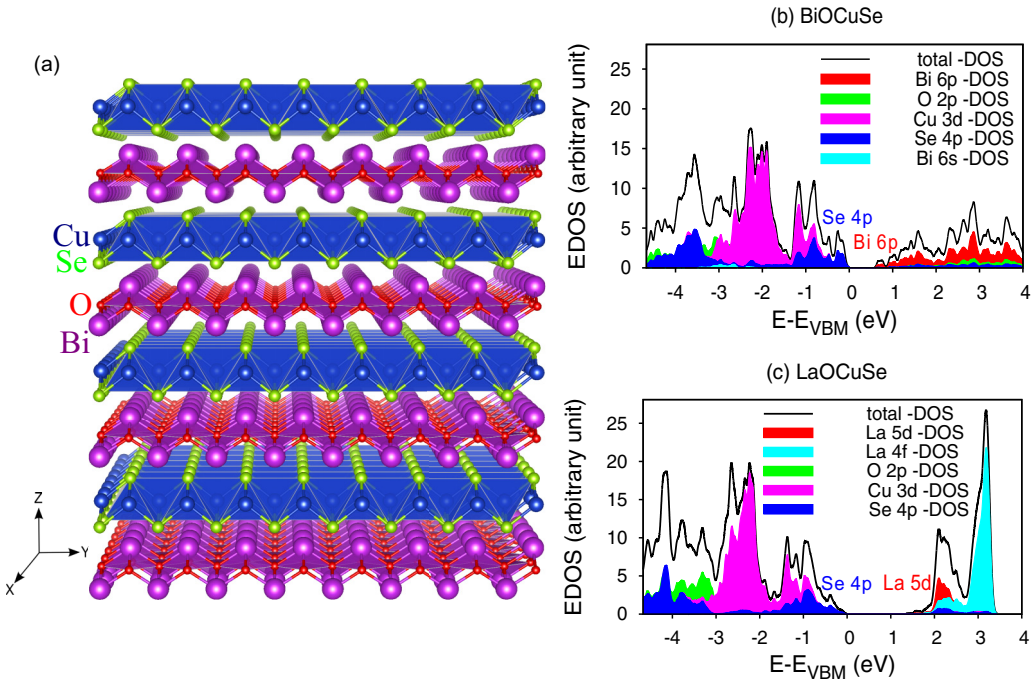

FIG. 1. (Color online) (a) The structural exquisiteness of a naturally occurring superlattice material BiCuSeO, adopting a quaternary ZrSiCuAs-type tetragonal structure ($P4/nmm$ space group). (b) Calculated EDOS of the valence and conduction band regions of BiOCuSe and (c) that of LaOCuSe; the energy axis is referenced with respect to the valence band maximum (VBM) and the major orbital contribution is highlighted.

Γ point, the factor group analysis yields

$$D_{4h}^{7} = A_{2u} \oplus E_u \qquad \text{(acoustic)}$$
$$\oplus\, 3A_{2u} \oplus 3E_u \oplus 2A_{1g} \oplus 2B_{1g} \oplus 4E_g \qquad \text{(optic)}.$$

Since the A_{1g}, B_{1g}, and E_g modes are Raman (R) active, there are eight Raman modes and since the A_{2u} and E_u modes are infrared (IR) active, there are six IR modes. From the analysis of eigendisplacements (see Table I), one can expect that the substitution of Se by another chalcogen atom should shift significantly the second A_{1g} Raman mode (∼176.6 cm^{-1}) and the third E_g Raman mode (∼158.0 cm^{-1}). Any defect or doping related to O atoms should modify the two higher-frequency B_{1g} (∼349.6 cm^{-1}) and E_g (∼417.6 cm^{-1}) Raman modes, whereas any defect or doping related to Cu atoms should change the lower-frequency B_{1g} Raman mode (∼110.1 cm^{-1}). The Cu atoms are involved also in the two lower-frequency E_g Raman modes (∼64.7 and 78.7 cm^{-1}). When going from BiOCuSe to LaOCuSe, the lower-frequency A_{1g} Raman mode (∼148.7 cm^{-1}) shifts to the higher-frequency A_{1g} Raman mode (∼199.8 cm^{-1}) due mainly to the fact that the latter has a lower mass. The Bi atoms are also involved in the two lower-frequency E_g Raman modes.

The longitudinal optical–transverse optical (LO-TO) splittings in the IR spectra for displacements parallel to the layers (in plane) occur for the E_{2u} modes and displacements parallel to the c axis (out of plane) occur for the A_{2u} modes. These splittings depend on BEC [34] and on the dielectric screening of the Coulomb interaction, determined by the electronic part of the DC [35]. For tetragonal symmetry as in MOCuSe, the BEC tensor $Z_s^{*\alpha\beta}$ is diagonal and reduces to two values, $Z_{xx}^* = Z_{yy}^* \equiv Z_{\parallel}^*$ and $Z_{zz}^* \equiv Z_{\perp}^*$, which show considerable anisotropy (see Table II). The values are significantly large for Bi, O, and La, suggesting that Bi-O and La-O bonds have a greater covalent character than Cu-Se bonds. The electronic dielectric permittivity tensor ε^{∞} describes the response of the electron gas to a homogeneous electric field if the ions are taken as fixed at their equilibrium positions [36]. The calculation gives $\varepsilon_{\parallel}^{\infty} = 18.01$ and $\varepsilon_{\perp}^{\infty} = 13.79$ for BiOCuSe (8.73 and 7.30 for LaOCuSe), corresponding to an ordinary optical refractive index, $n_o = 4.24$, and an extraordinary refractive index $n_e = 3.71$ for BiOCuSe (2.95 and 2.70 for LaOCuSe). Due to the difference between the calculated and measured band-gap energies, these values are expected to be somewhat larger than the experimentally measured values, which are not yet available in the literature. Table II shows that the lattice contribution to the in-plane dielectric response ($\varepsilon_{\parallel}^{0} - \varepsilon_{\parallel}^{\infty}$) is quite larger in BiOCuSe than in LaOCuSe, which indicates the presence of a lower-frequency phonon in the former than in the latter and is consistent with the fact that the Bi atom is heavier than the La atom.

Figure 2 shows the phonon dispersion curves and DOS of BiOCuSe and LaOCuSe. In both materials, the vibrations of O are decoupled from those of other atoms and occupy the high-frequency region above about 250 cm^{-1} while the latter occupy the low-frequency region below about 200 cm^{-1}. For the same structure, the mass homology relation can be applied to describe the mode frequency difference, at least for the low-frequency modes where interatomic force (IF) constants hardly change; however, for the high-frequency modes, the

TABLE I. Calculated optical phonon frequencies of BiOCuSe and LaOCuSe at the high-symmetry point Γ along with their mode symmetries, characters, activities, pressure coefficients, and descriptions of involved atoms in the eigendisplacements [32]. The frequency values are compared with the experimentally obtained IR data from the literature [33] (when available).

BiOCuSe					LaOCuSe			
	ω (cm^{-1})		$\frac{\partial\omega}{\partial P}$			ω	$\frac{\partial\omega}{\partial P}$	
Mode	DFT	Expt. [33]	(cm^{-1}/GPa)	Involved atoms; direction	Mode	(cm^{-1})	(cm^{-1}/GPa)	Involved atoms; direction
E_u(IR,TO1)	53.0	59.5	3.71	All (mostly Cu, leastly O); y	E_g(R,1)	62.0	2.78	All (mostly Cu, leastly O); x and y
E_u(IR,LO1)	61.2		2.81	All (mostly Cu, leastly O); x	E_u(IR,TO1)	72.2	3.33	All (mostly Cu, leastly Se); y
E_g(R,1)	64.7		1.08	All (mainly Cu and Bi); x and y	E_u(IR,LO1)	75.2	3.25	All (mostly Cu, leastly Se); x
A_{2u}(IR,TO1)	75.9		2.61	All (mostly Se, leastly O); z	A_{2u}(IR,TO1)	90.2	3.09	All (mostly Cu, leastly O); z
E_g(R,2)	78.7		2.83	All (mostly Cu, leastly O); x and y	A_{2u}(IR,LO1)	102.1	3.03	All (mostly Cu, leastly Se); z
A_{2u}(IR,LO1)	89.4	92.0	2.38	All (mostly Se, leastly O); z	B_{1g}(R,1)	115.7	3.40	Only Cu (more) and O (much less); z
E_u(IR,TO2)	101.0	116.5	5.23	All (mostly Se, leastly Bi); y	E_g(R,2)	121.9	1.81	All (mostly La, leastly Se); x
B_{1g}(R,1)	110.1		3.46	Only Cu (more) and O (much less); z	E_u(IR,TO2)	130.5	5.06	All (mostly Se, leastly O); y
E_u(IR,LO2)	142.7		4.29	All (mostly Se, leastly Bi); x	E_u(IR,LO2)	152.5	5.20	All (mostly Se, leastly La); x
A_{1g}(R,1)	148.7		4.48	Only Bi (more) and Se (less); z	A_{2u}(IR,TO2)	153.5	3.85	All (mostly Cu, leastly La); z
A_{2u}(IR,TO2)	149.8		1.61	All (mostly Cu, leastly Bi); z	A_{1g}(R,1)	171.6	4.18	Only Se (more) and La (less); z
E_g(R,3)	158.0		4.62	All (mostly Se, leastly Bi); x and y	A_{2u}(IR,LO2)	172.3	3.90	All (mostly Se, leastly O); z
A_{1g}(R,2)	176.6		2.98	Only Se (more) and Bi (less); z	E_g(R,3)	172.4	4.54	All (mostly Se, leastly O); x and y
A_{2u}(IR,LO2)	178.6		3.53	All (mostly Se, leastly O); z	A_{1g}(R,2)	199.8	1.94	Only La (more) and Se (less); z
E_u(IR,TO3)	264.7	262.0	5.31	Mostly O, others slightly; y	B_{1g}(R,2)	306.5	3.55	Only O (more) and Cu (much less); z
E_u(IR,LO3)	347.7		6.65	Mostly O, others slightly; x	E_u(IR,TO3)	311.2	4.53	All (mostly O, leastly Cu); y
B_{1g}(R,2)	349.6		4.97	Only O (more) and Cu (much less); z	E_u(IR,LO3)	402.3	4.19	All (mostly O, leastly Cu); x
A_{2u}(IR,TO3)	397.9	390.0	4.70	Mostly O, others slightly; z	A_{2u}(IR,TO3)	436.0	3.22	All (mostly O, leastly Cu); z
E_g(R,4)	417.6		5.34	Mostly O, others slightly; x and y	E_g(R,4)	437.4	4.34	All (mostly O, leastly Cu); x and y
A_{2u}(IR,LO3)	473.7	475.0	5.86	Mostly O, others slightly; z	A_{2u}(IR,LO3)	531.9	4.07	All (mostly O, leastly Cu); z

TABLE II. Calculated Born effective (Z^*) and nominal charges (Z^n), optical (ε^∞) and static (ε^0) dielectric constants, longitudinal (v_l), transverse (v_t), and average (v_a) sound velocities (in m/s), Debye temperature (Θ_D, in K), and Grüneisen parameter (γ) for BiOCuSe and LaOCuSe in their $P4/nmm$ phase.

	$Z^*_{M_\perp}$	$Z^*_{M_\parallel}$	Z^n_M	$Z^*_{O_\perp}$	$Z^*_{O_\parallel}$	Z^n_O	$Z^*_{Cu_\perp}$	$Z^*_{Cu_\parallel}$	Z^n_{Cu}	$Z^*_{Se_\perp}$	$Z^*_{Se_\parallel}$	Z^n_{Se}	$\varepsilon^\infty_\perp$	$\varepsilon^\infty_\parallel$	$\varepsilon^0_\perp$	$\varepsilon^0_\parallel$	v_l	v_t	v_a	Θ_D	γ
BiOCuSe	5.93	6.46	3	−4.42	−4.28	−2	1.06	1.44	2	−2.70	−3.67	−3	13.79	18.01	22.64	83.34	4095.1	2139.8	2393.8	277	1.85
LaOCuSe	4.87	4.68	3	−3.70	−3.19	−2	0.41	1.04	2	−1.72	−2.58	−3	7.30	8.73	17.57	21.70	4590.7	2518.0	2807.6	322	1.68

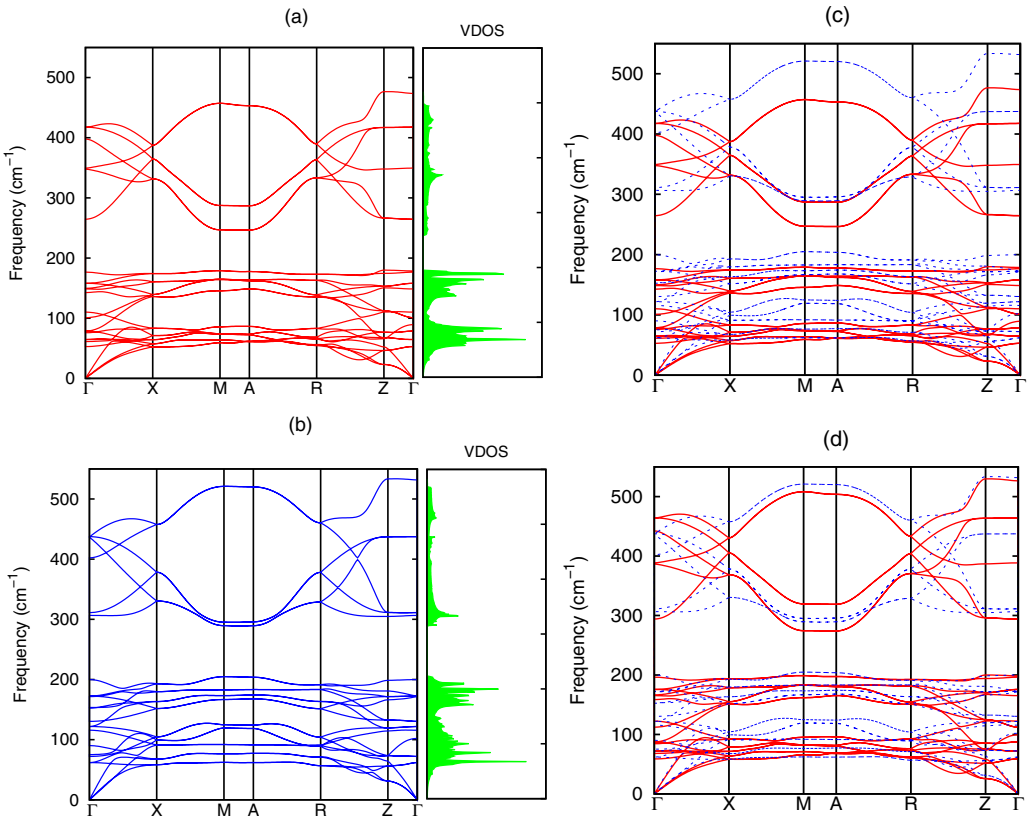

FIG. 2. (Color online) Calculated phonon dispersion and DOS of (a) BiOCuSe and (b) LaOCuSe along the high-symmetry lines of the Brillouin zone. (c) Calculated phonon dispersion curves of both materials for a direct comparison; solid (red) lines for BiOCuSe and dashed (blue) lines for LaOCuSe. (d) Calculated original phonon dispersion data of BiOCuSe [from (a)], multiplied by 1.1116 (see text) are plotted using solid (red) lines for a comparison with the original [from (b)] LaOCuSe dispersion data, plotted now using dashed (blue) lines.

changes in the IF constants are expected to be large. The mass of the unit cell $M_{\rm uc}$ changes from 734.9716 amu for BiOCuSe to 594.8217 amu for LaOCuSe, by a factor of 1.2356. Therefore, the mode frequencies can be increased by a factor of $\sqrt{1.2356} = 1.1116$ if replacing the mass of Bi by that of La. The original BiOCuSe dispersion, multiplied by 1.1116, is shown in Fig. 2(d). Such scaling is sufficient to describe the change in the low-frequency part of the phonon dispersion. In particular, the low-frequency acoustic modes obtained in this way match well with those for LaOCuSe, which means the change of low-frequency acoustic phonons or equivalently, the change of sound velocities, is almost entirely due to the mass decrease from Bi to La.

The propagation velocities of longitudinal (v_l) and transverse (v_t) acoustic waves are derived from the slope of the acoustic phonon dispersion in the low-q limit (see Table II). The Debye temperature (Θ_D) [37] is calculated from the relation $\Theta_D = \frac{h}{k_B}(\frac{3n}{4\pi\Omega})^{1/3} v_a$, where h and k_B are Planck and Boltzmann constants, respectively, n is the number of atoms in the cell, Ω is cell volume, and v_a is the average sound wave velocity. The v_a, obtained [by Eq. (7) in Ref. [17]] using theoretical v_l and v_t provided in Table II , is in reasonable [38] agreement with the experimentally measured value of 2112 m/s for BiOCuSe [20]. The v_l and v_t are essentially harmonic parameters while their ratio v_l/v_t is an anharmonic quantity which depends on the ratio between the axial and shear rigidities of interatomic bonds and thus is related [see Eqs. (10) and (11) in Ref. [17]] to the Grüneisen parameter γ, which suggests the degree of anharmonicity [39,40].

Finally, the most striking result of this study is the crossing of the low-frequency mode when one goes from LaOCuSe to BiOCuSe. In BiOCuSe, the lowest-frequency optical (LFO) mode E_u(IR,TO1) has E_u symmetry, the same as its acoustic modes, and behaves as a quasiacoustic mode, whereas in LaOCuSe the LFO mode E_g(R,1) has E_g symmetry [see Fig. 3(a)]. This symmetry matching as well as a lower value of the LFO mode in BiOCuSe than in LaOCuSe clearly suggest that the acoustic modes can interact more strongly or can be hybridized more strongly in the former than in the latter, leading to a larger acoustic-optical phonon scattering and hence lower κ. Additionally, despite being very heavy, Bi atoms in the E_u(IR,TO1) mode [see Fig. 3(a)] exhibit a significantly large displacement, indicating higher anharmonic effects. Indeed, as the E_u(IR,TO1) mode in BiOCuSe has a larger mode Grüneisen parameter γ_j [42] than the E_g(R,1) mode in LaOCuSe [see Fig. 3(b)], the anharmonicity for the former is larger, leading to a stronger anharmonic scattering at elevated temperatures [43]. At high temperatures, for nonmetallic crystalline solids, the anharmonic umklapp processes are dominant in scattering heat-conducting phonons. Assuming

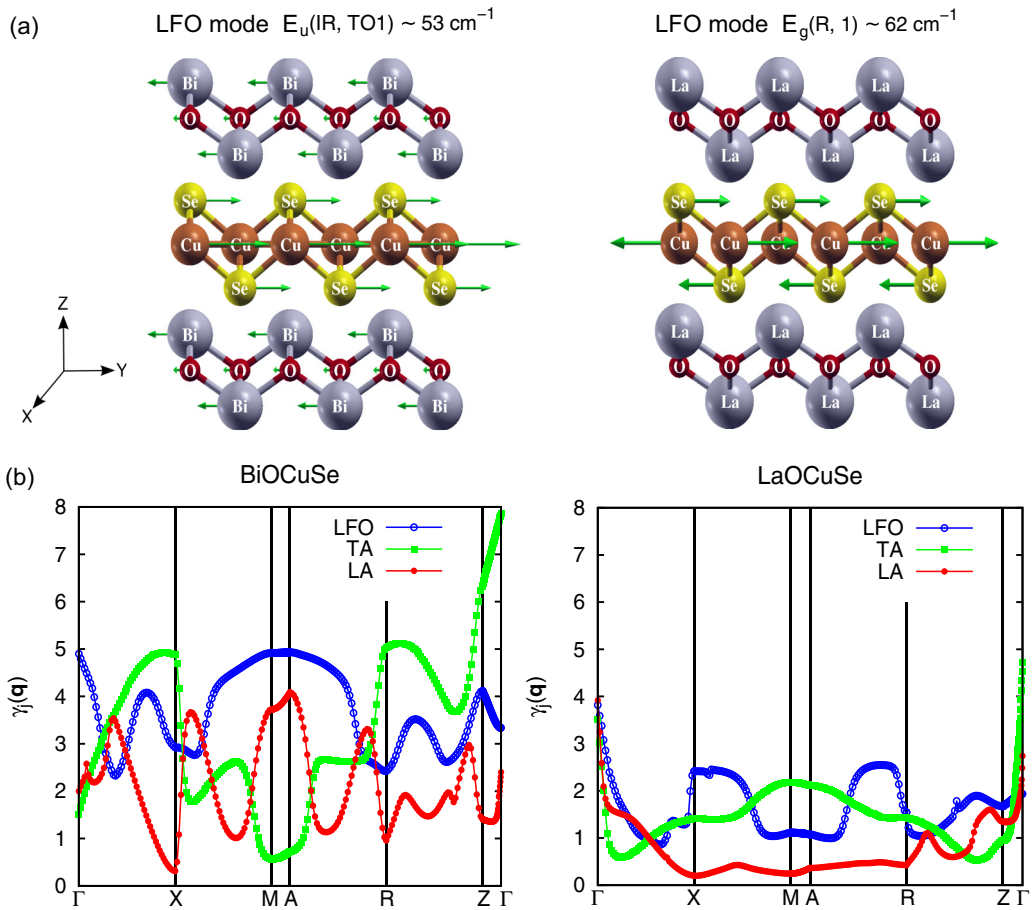

FIG. 3. (Color online) (a) Atomic displacement patterns for the respective lowest-frequency optical (LFO) mode, i.e., E_u(IR,TO1) ~ 53 cm^{-1} in BiOCuSe (left panel) and E_g(R,1) ~ 62 cm^{-1} in LaOCuSe (right panel). Arrows are proportional to the amplitude of the atomic motions. (b) Mode Grüneisen dispersion of the above LFO mode in comparison to that of the longitudinal acoustic (LA) and transverse acoustic (TA) modes in BiOCuSe (left panel) and in LaOCuSe (right panel), respectively. In both panels, open circles (blue), solid circles (red), and solid squares (green) stand for LFO, LA, and TA modes.

the heat is conducted only by acoustic and quasiacoustic phonons via these umklapp scattering processes, the thermal conductivity can be evaluated by [44] $\kappa = 3.1 \times 10^{-6} \frac{\bar{M}\Theta_D^3 \delta}{\gamma_\alpha^2 n^{2/3} T}$ in W m^{-1}K^{-1}, where $\bar{M}$ is the average atomic mass in amu, Θ_D is the Debye temperature in K, δ^3 is the volume per atom in Å^3, n is the number of atoms in the primitive unit cell, and γ_α is the average acoustic and quasiacoustic mode Grüneisen parameter. This relation gives $\kappa = 0.5$ W m^{-1}K^{-1} at $T = 923$ K for BiOCuSe with $\gamma_\alpha = 2.9$, whereas $\kappa = 1.9$ W m^{-1}K^{-1} at $T = 923$ K for LaOCuSe with $\gamma_\alpha = 1.9$. The κ of BiOCuSe is calculated to be about four times lower than that of its isostructural analog LaOCuSe using the present PBEsol estimates of the above parameters. This result is in good agreement with the experimental observation [19]. Furthermore, the calculated out-of-plane γ_α [$\gamma_\alpha^\perp$ or $\gamma_\alpha(\Gamma Z)$] in BiOCuSe [as obtained from Fig. 3(b), left panel] is found to be about two times larger than in-plane γ_α [$\gamma_\alpha^\parallel$ or $\gamma_\alpha(\Gamma X)$], resulting in that the out-of-plane thermal conductivity (κ_{zz}) in BiOCuSe is about two times smaller ($\kappa_{zz} \approx 0.31$ W m^{-1}K^{-1} at $T = 923$ K) than the in-plane one ($\kappa_{xx} \approx 0.6$ W m^{-1}K^{-1} at $T = 923$ K). This suggests that BiOCuSe has an unprecedented twofold anisotropy of heat flow between the in-plane and out-of-plane directions.

In conclusion, a first-principles DFT study of the lattice dynamics and related properties of BiOCuSe and LaOCuSe is performed to find the reasons why BiOCuSe is a better thermal insulator than LaOCuSe. For these oxychalcogenides, phonon frequencies with symmetries, characters, spectroscopic activities, displacement patterns, and pressure coefficients of different zone-center modes, dielectric constants, dynamical charges, and phonon and Grüneisen dispersions are determined, which will certainly motivate future experimental studies, especially in IR and Raman spectroscopies. Despite their similar Young's modulus values, the material with a heavier element is found to exhibit lower κ as the higher atomic mass produces lower phonon frequencies, slower sound velocities, and a higher average mode Grüneisen parameter, which are more detrimental to heat transfer. This theoretical study is likely to be of value for the development of advanced TE technologies based on this class of oxychalcogenide thermoelectrics.

[1] L. D. Zhao, D. Berardan, Y. L. Pei, C. Byl, L. Pinsard-Gaudart, and N. Dragoe, Appl. Phys. Lett. **97**, 092118 (2010).
[2] C. Wood, Energy Convers. Manage. **24**, 317 (1994).
[3] G. J. Snyder and E. S. Toberer, Nat. Mater. **7**, 105 (2008).
[4] T. C. Harman, P. J. Taylor, M. P. Walsh, and B. E. LaForge, Science **297**, 2229 (2002).
[5] J. P. Heremans, C. M. Thrush, and D. T. Morelli, Phys. Rev. B **70**, 115334 (2004).
[6] J. P. Heremans, V. Jovovic, E. S. Toberer, A. Saramat, K. Kurosaki, A. Charoenphakdee, S. Yamanaka, and G. J. Snyder, Science **321**, 554 (2008).
[7] K. F. Hsu, S. Loo, F. Guo, M. W. Chen, J. S. Dyck, C. Uher, T. Hogan, E. K. Polychroniadis, and M. G. Kanatzidis, Science **303**, 818 (2004).
[8] B. Poudel, Q. Hao, Y. Ma, Y. Lan, A. Minnich, B. Yu, X. Yan, D. Wang, A. Muto, D. Vashaee, X. Chen, J. Liu, M. S. Dresselhaus, G. Chen, and Z. F. Ren, Science **320**, 634 (2008).
[9] L. D. Zhao, B. P. Zhang, J. F. Li, M. Zhou, W.-S. Liu, and J. Liu, J. Alloys Compd. **455**, 259 (2008).
[10] L. D. Zhao, S. Lo, J. J. He, H. Li, K. Biswas, J. Androulakis, C. I. Wu, T. P. Hogan, D. Y. Chung, V. P. Dravid, and M. G. Kanatzidis, J. Am. Chem. Soc. **133**, 20476 (2011).
[11] K. Biswas, J. He, I. D. Blum, C. I. Wu, T. P. Hogan, D. N. Seidman, V. P. Dravid, and M. G. Kanatzidis, Nature (London) **489**, 414 (2012).
[12] K. Biswas, J. He, Q. Zhang, G. Wang, C. Uher, V. P. Dravid, and M. G. Kanatzidis, Nat. Chem. **3**, 160 (2011).
[13] L. D. Zhao *et al.*, J. Am. Chem. Soc. **134**, 16327 (2012).
[14] J. Sui *et al.*, Energy Environ. Sci. **6**, 2916 (2013).
[15] Y. Liu, L. D. Zhao, Y. Liu, J. Lan, W. Xu, F. Li, B. P. Zhang, D. Berardan, N. Dragoe, Y. Lin, C. Nan, J. F. Li, and H. Zhu, J. Am. Chem. Soc. **133**, 20112 (2011).
[16] J. Li, J. H. Sui, Y. L. Pei, C. Barreteau, D. Berardan, N. Dragoe, J. Q. He, and L. D. Zhao, Energy Environ. Sci. **5**, 8543 (2012).
[17] Y. L. Pei, J. He, J. F. Li, F. Li, Q. Liu, W. Pan, C. Barreteau, D. Berardan, N. Dragoe, and L. D. Zhao, NPG Asia Mater. **5**, e47 (2013).
[18] In addition, compared to the state-of-the-art TE materials, e.g., PbTe and Bi_2Te_3, such oxyselenides have advantages in chemical and thermal robustness, cost effectiveness, and environmental compatibility [16].
[19] M. Yasukawa, K. Ueda, and H. Hosono, J. Appl. Phys. **95**, 3594 (2004).
[20] F. Li, J. F. Li, L. D. Zhao, K. Xiang, Y. Liu, B. P. Zhang, Y. H. Lin, C. W. Nan, and H. M. Zhu, Energy Environ. Sci. **5**, 7188 (2012).
[21] This can be partly, if not entirely, due to the fact that the presence of heavy elements in such a layered oxyselenide leads to certain low-frequency phonons which are very hard to converge numerically and require computationally expensive tight tolerance criteria.
[22] All calculations are performed using the QUANTUM ESPRESSO [23,24] implementation of DFT, with the PBEsol exchange-correlation functional, projector augmented-wave (PAW) potential [25,26], and a 50 Ry energy cutoff. Phonon frequencies are calculated using density functional perturbation theory (DFPT) [27] at the level of linear response, which allows exact (within DFT) computations of phonon frequencies at any point in the Brillouin zone. The Brillouin zone integrations are done on a uniform Monkhorst-Pack **k** grid of $11 \times 11 \times 5$.
[23] S. Baroni, S. de Gironcoli, A. Dal Corso, and P. Giannozzi, http://www.pwscf.org.
[24] A. Aravindh *et al.*, Solid State Commun. **144**, 273 (2007).
[25] A. Dal Corso, Comput. Mater. Sci. **95**, 337 (2014).
[26] S. K. Saha, S. Manna, M. Przybylski, V. S. Stepanyuk, and J. Kirschner, Phys. Rev. B **90**, 081404(R) (2014).
[27] S. Baroni, S. de Gironcoli, A. Dal Corso, and P. Giannozzi, Rev. Mod. Phys. **73**, 515 (2001).
[28] The atomic positions are as follows: M, $2c(1/4,1/4,z_M)$; O, $2a(3/4,1/4,0)$; Cu, $2b(3/4,1/4,1/2)$; and Se, $2c(1/4,1/4,z_{Se})$, where z_M and z_{Se} are the so-called internal coordinates. In this natural superlattice structure, the antifluoritelike $(Cu_2Se_2)^{2-}$ chalcogenide layers of slightly distorted edge-sharing $CuSe_4$ tetrahedra alternate with fluoritelike $(M_2O_2)^{2+}$ oxide layers, stacked along the c axis of the tetragonal cell.
[29] E. S. Stampler, W. C. Sheets, M. I. Bertoni, W. Prellier, T. O. Mason, and K. R. Poeppelmeier, Inorg. Chem. **47**, 10009 (2008).
[30] K. Ueda and H. Hosono, J. Appl. Phys. **91**, 4768 (2002).
[31] The band gap of BiOCuSe is narrower than that of LaOCuSe, mainly due to the unoccupied low-energy Bi $6p$ orbitals which are not present in LaOCuSe. For both systems, the top of the valence-band region is primarily of Cu $3d$ and Se $4p$ character, with the majority of the O $2p$ orbital lying $\sim$3 eV below the valence band maximum (VBM). In the vicinity of the VBM of BiOCuSe, the contribution of the Bi $6s$ orbitals is not large, and Bi $6s$ states are mostly located deep in the valence band (-9 to -12 eV relative to the VBM). The conduction band minimum (CBM) of BiOCuSe mainly consists of Bi $6p$ states whereas that of LaOCuSe is mainly composed of La $5d$ and Cu $4s$ orbitals. It is noteworthy that, in the vicinity of the VBM (0 to -0.6 eV), Cu and Se contribute almost equally to the DOS, and synergistically determine the electronic conduction.
[32] The directions of the displacements are in plane for the E modes and out of plane for the A modes.
[33] P. S. Berdonosov, A. M. Kusainova, L. N. Kholodkovskaya, V. A. Dolgikh, L. G. Akselrud, and B. A. Popovkin, J. Solid State Chem. **118**, 74 (1995).
[34] The BEC tensor $Z_s^{*\alpha\beta}$ is the first derivative of the macroscopic polarization along the α direction with respect to the displacement of sth atom along the β direction. This dynamical quantity is strongly influenced by dynamical changes of orbital hybridization induced by atomic displacements.
[35] G. Dutta, S. K. Saha, and U. V. Waghmare, Solid State Commun. **150**, 2020 (2010).
[36] K. L. Kostov, S. Polzin, S. K. Saha, O. Brovko, V. Stepanyuk, and W. Widdra, Phys. Rev. B **87**, 235416 (2013).
[37] P. Debye, Ann. Phys. **39**, 789 (1912).
[38] The difference between theory and experiment can be attributed to the difference in lattice parameters arising from thermal effects, or/and to the uncertainty in ultrasonic pulse echo measurement.
[39] D. S. Sanditov, A. A. Mashanov, and M. V. Darmaev, Tech. Phys. **54**, 1398 (2009).
[40] A larger γ indicates higher anharmonicities of the chemical bond which generally drives greater phonon-phonon scatterings (umklapp or/and normal) and thus shorter relaxation times [41].

[41] A. F. Ioffe, *Physics of Semiconductors* (Infosearch, London, 1958).

[42] The Grüneisen parameter of the $(j,\mathbf{q})$-phonon mode is defined as $\gamma_j(\mathbf{q}) = -\frac{V}{\omega_j(\mathbf{q})}\frac{\partial\omega_j(\mathbf{q})}{\partial V}$ and is calculated using the finite difference approach by computing phonon dispersion curves at two perturbed structures that are obtained from the equilibrium structure by straining the volume by $\pm 1.5\%$ and reoptimizing the atomic positions.

[43] M. Di Gennaro, S. K. Saha, and M. J. Verstraete, Phys. Rev. Lett. **111**, 025503 (2013).

[44] G. A. Slack, J. Phys. Chem. Solids **34**, 321 (1973).